Pergamon

Journal of Structural Geology, Vol. 17, No. 8, pp. 1139 to 1149, 1995

0191-8141/95 $9.50+0.00

0191-8141(95)00008-9

The influence of pre-existing thrust faults on normal fault geometry in nature and in experiments

CLAUDIO FACCENNA,* THIERRY NALPAS, JEAN-PIERRE BRUN and PHILIPPE DAVY

Geosciences Rennes UPR4661 CNRS, Campus de Beaulieu, Université de Rennes I, 35042 Rennes Cedex, France

and

VITTORIO BOSI

Istituto Nazionale di Geofisica, Via di Vigna Murata 605, 00143 Roma, Italy

(*Received* 4 *January* 1994; *accepted in revised form* 23 *December* 1994)

Abstract—Relations between normal faults and pre-existing thrust faults are classically described in terms of three basic situations: normal faults can cross-cut thrust faults; they can branch out from thrust faults at depth on a décollement level, or they can entirely reactivate thrust planes. The mechanical aspects of these types of interaction were studied by analogue modelling in which sand simulates the 'brittle' rocks and silicone putty an interlayered décollement. The models underwent compression, producing thrust faults with variable dips, followed by extension. Three possible ways of interaction are described here: (a) *no interaction* occurs in the case of low-dip thrust faults (<32° ± 1°) and normal faults are developed independently, displaying a listric geometry; (b) *branching at depth* on the décollement level occurs when dip of the thrust faults reaches 32° ± 1°. In this case, the dip of the normal faults, whose geometry becomes planar, decreases with increasing thrust dip. We suggest that this change in dip of normal faults depends upon the rotation of stress tensor axes along the pre-existing fault zone, where a drop in the friction coefficient is likely to occur; (c) *reactivation* occurs in brittle material when dip of the pre-existing fault exceeds 41° ± 1°.

INTRODUCTION

The way in which normal faults interact with pre-existing crustal anisotropies such as thrust planes is a crucial topic in understanding extensional processes. It is generally accepted that pre-existing thrust systems exert an influence on the geometry (location, dip and direction) of the newly-formed normal faults, even if the thrust planes are partially—if at all—reactivated (Allmendinger *et al.* 1983, Brun & Choukroune 1983, Smith & Bruhn, 1984, Malavielle 1987, Seranne & Seguret 1987, Powell & Williams 1989, Jolivet *et al.* 1991). The geometrical relationship and/or interaction between normal faults and pre-existing thrust planes can be summarized in terms of three basic situations (Williams *et al.* 1989) (Fig. 1):

(a) normal faults may cross-cut and offset the pre-existing thrust planes (Fig. 1a) (Wernicke 1981, Powell & Williams 1989).

(b) Normal faults may branch out from thrust faults at depth on a weak fault zone or on a décollement level (Fig. 1b), as often observed in the North Sea region (Stoneley 1982, Chadwick *et al.* 1983, Brewer & Smythe 1984, Cheadle *et al.* 1987, Enfield & Coward 1987, Gibbs 1987, Stein & Blundell 1990).

(c) Pre-existing thrust planes may be entirely (Fig. 1c) (Ratcliffe *et al.* 1986) or partially reactivated, as suggested for ramp and flat thrust geometries (Petersen *et al.* 1984, Smith & Bruhn 1984, Arabasz & Julander 1986,

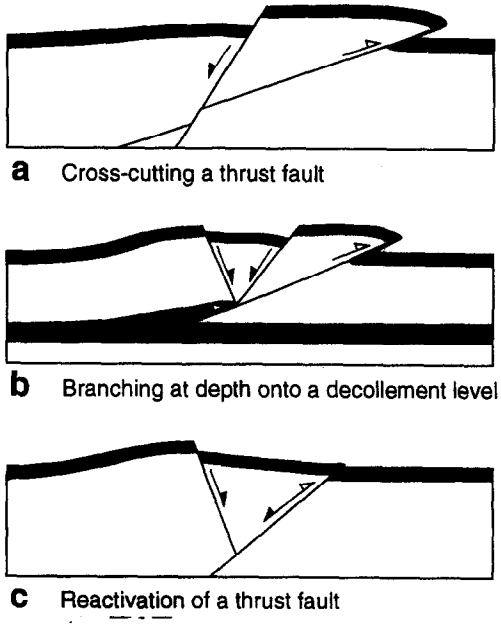

Fig. 1. Three basic geometries summarizing the possible relations between normal faults and pre-existing thrust faults. Grey ornamentation indicates a décollement level. For references and other details see text.

*Present address: Dipartimento di Scienze Geologiche, III Università di Roma, Via Ostiense 169, 00154 Roma, Italy.

Cooper & Burbi 1986, Powell & Williams 1989, Williams *et al.* 1989, Gorini *et al.* 1991).

From a mechanical point of view, reactivation processes occur because pre-existing fault zones are generally weaker than the unfracturated surrounding rocks. Three critical weakness parameters are commonly invoked: a drop in cohesion between the fault zone and its surrounding rocks (Donath & Cronwell 1981, Huyghe & Mugnier 1992), a drop in friction coefficient (Ivins *et al.* 1990) and high pore-pressures within the fault zone (Hubbert & Rubey 1959, Sibson 1985, Ivins *et al.* 1990, Sibson, 1990). These three parameters induce a drop in shear strength along the pre-existing structure, thus limiting reactivation to faults that are properly oriented with respect to the subsequent principal stress directions (Ivins *et al.* 1990, Ranalli & Yin 1990, Yin & Ranalli 1992).

The aim of this paper is to study the geometry of the normal faults as a function of pre-existing crustal anisotropies using small-scale models. The style of the models is based on the geometries observed in two natural examples, from the Apennines and from the North Sea region.

TWO GEOLOGICAL EXAMPLES

It is beyond the scope of the paper to carry out a through review of the extensional reactivation of thrust faults. Several papers (see references above) treat this topic. Our aim is to present field and seismic evidence of the extensional reactivation of thrust faults. The two examples studied here provide evidence for the role of thrust fault dip and décollement on the reactivation of thrust faults and on the location of newly formed normal faults.

Central Apennines (Italy)

Two main tectonic phases, first compressional (Miocene–Pliocene) and then extensional (Pliocene to recent) have traditionally been recognized in the central part of the Apennine chain (Parotto & Praturlon 1975, Funiciello *et al.* 1981). These tectonic phases at first produced stacking of the Meso-Cenozoic sedimentary sequences via NW–SE-striking thrust planes, and then extensional collapse with northwest–southeast normal faults and asymmetric basins (Fig. 2a). In this terrain, extensional reactivation of thrust faults is widely recognized and accepted as a suitable mechanism, acting both on superficial thrust faults (Cooper & Burbi 1986) and on deep décollement levels (Bally *et al.* 1986, Lavecchia *et al.* 1987, Ghisetti *et al.* 1993).

Detailed structural and geological studies along part of a 40 km long northwest–southeast fault zone, described as an example of a reactivated thrust fault (Fig. 2a) (Nijman 1971, Mariotti & Capotorti 1988, Bosi *et al.* in press), have been performed in order to acquire some insight into the geometrical aspects of reactivation. In this area, compression developed during the Late Miocene–Early Pliocene with high- and low-angle imbricated thrust faults affecting carbonate and terrigenous sequences (Fig. 2b). Thin layers of clay, marl and sand are often intercalated inside the fault zone between the carbonate walls. A subsequent early Pleistocene extensional phase induced the reactivation of high-angle thrust faults and the formation of new normal faults parallel to the thrust planes (Fig. 2b). The attitude and the kinematics of the studied fault planes were recognized in the field by means of kinematic analysis and by geometrical reconstructions; in particular, the extensional reactivation of pre-existing thrust planes was inferred from stratigraphical criteria and by the superposition of slickensides on the same fault plane on mesoscopic and microscopic scale (details in Bosi *et al.* in press). Extensional reactivation has been observed mainly for 37°–40° and for 35°–37° dipping thrust planes, with a minimum normal offset of 500 m (Fig. 2c) (Nijman 1971, Bosi *et al.* in press). On the contrary, shallow dipping thrust planes (31° and 16°–21°) do not display any evident traces of reactivation and are locally cut by newly-formed normal faults (dipping 57°–65°) (Fig. 2c). On the basis of these data, we suggest that extensional reactivation in this region is more frequent for high-angle than for low-angle thrust faults.

Broad Fourteens Basin (North Sea)

A good example of extensional reactivation of a thrust fault at depth—above a décollement level—is provided by the northwestern border of the Broad Fourteens Basin (BFB), which is located off the coast of the Netherlands on the southern edge of a Permian evaporite basin (Ziegler 1975) (Fig. 3a). In order to point out the structural relationship between pre-existing Upper Cretaceous thrust planes and Tertiary normal faults, a detailed analysis of seismic profiles along the western border of the BFB has been carried out (Nalpas 1994). The thrust system involves a significant component of dextral strike-slip motion and detaches—via the salt layer—the sedimentary cover from the basement (Bodenhausen & Ott 1981, Nalpas *et al.* in press). In the investigated area (Fig. 3b), thrust planes dip to the east-northeast. Normal faults are systematically located just behind the thrust tip, branching out from the termination of the salt décollement level (Fig. 3c). This example indicates that the presence of a thrust plane connected to a basal décollement level is able to control the location of normal faults. Branching at depth on the thrust plane occurs preferentially at the top of the décollement level.

ANALOGUE MODELLING

Experimental procedure

Models were performed to simulate geological situations comparable to those described before. The modelling techniques are similar to those commonly used for

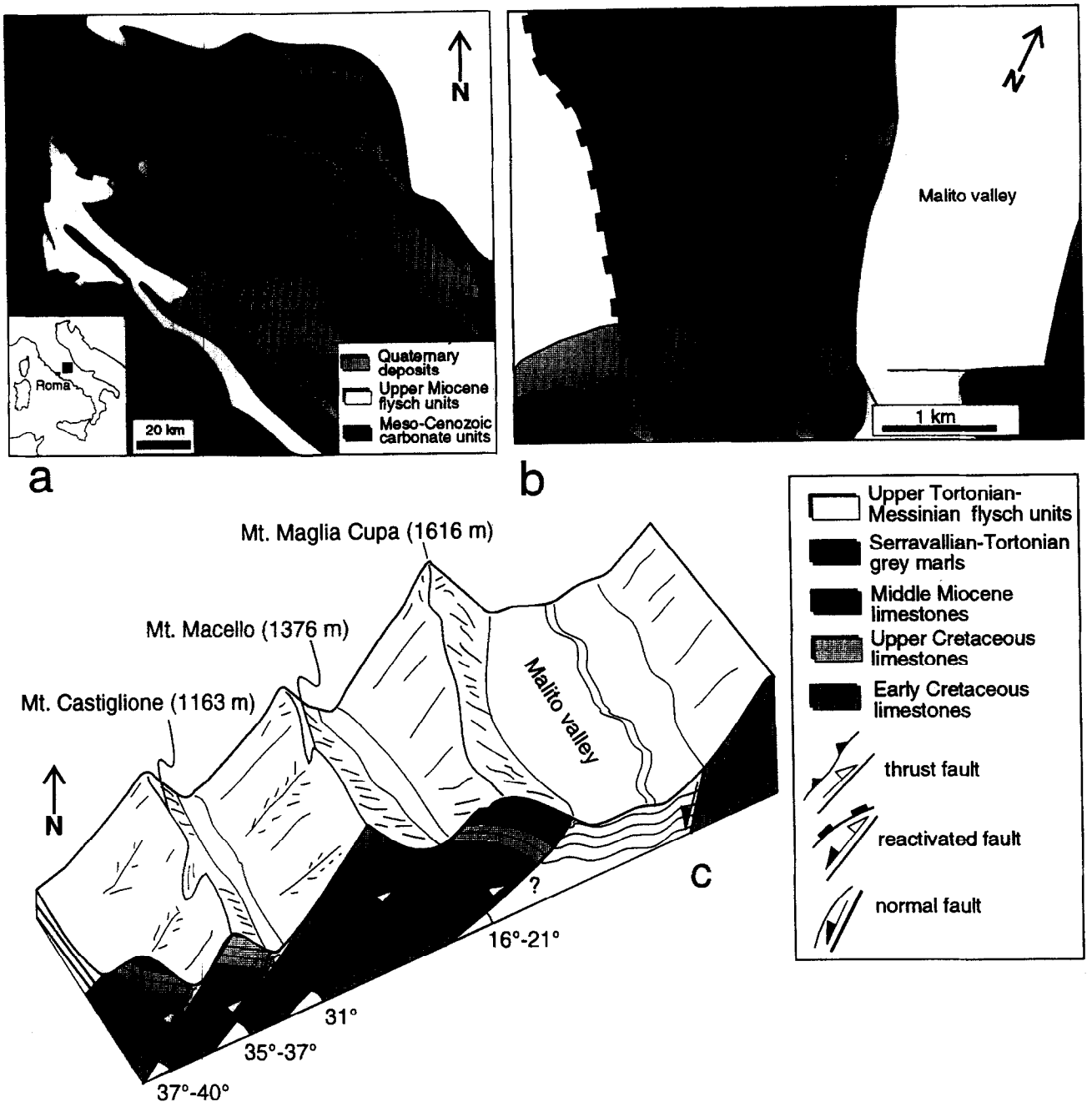

Fig. 2. Example of extensional reactivation of pre-existing thrust planes in the Central Apennines. (a) Simplified structural map of the Central Apennines (modified after Funiciello *et al.* 1981); (b) structural map of a part of the studied area; (c) schematic block diagram, not to scale (modified from Bosi *et al.* in press).

experiments on brittle–ductile systems at the Laboratory of Experimental Tectonics of the Geosciences Department (Rennes) (e.g. Vendeville *et al.* 1987, Allemand *et al.* 1989, Davy & Cobbold 1991, Nalpas & Brun 1993). The brittle behaviour of upper crustal rocks is simulated by dry sand and the ductile behaviour of the décollement layer (e.g. salt level) is simulated by silicone putty. The rheological properties of the materials have been described previously by Mandl *et al.* (1977), Davy (1986), Weijermars (1986), Davy & Cobbold 1991, Krantz (1991a). Parameters for sand are given in the Appendix; the materials and experimental parameters used in the present study are summarized in Table 1.

The deformation apparatus is made up of a mobile basal plate attached to a vertical end wall, sliding at a constant velocity along an underlying fixed basal plate (Fig. 4). The displacement is applied by means of two screw jacks, which are fixed onto the mobile plate, thus inducing a velocity discontinuity at the base of the model. The velocity discontinuity (VD) induces the formation of faults in the central part of the model in order to simulate a deep crustal anisotropy.

Two sets of experiments were carried out. In the first one, faulting is developed within a single brittle layer (set I of Fig. 4a and Table 1); in the second, the models involve an interlayered shallow-dipping (5°–6°) and viscous décollement layer (set II of Fig. 4b and Table 1). The dip-angle chosen for the décollement layer corresponds to the average décollement angle observed in

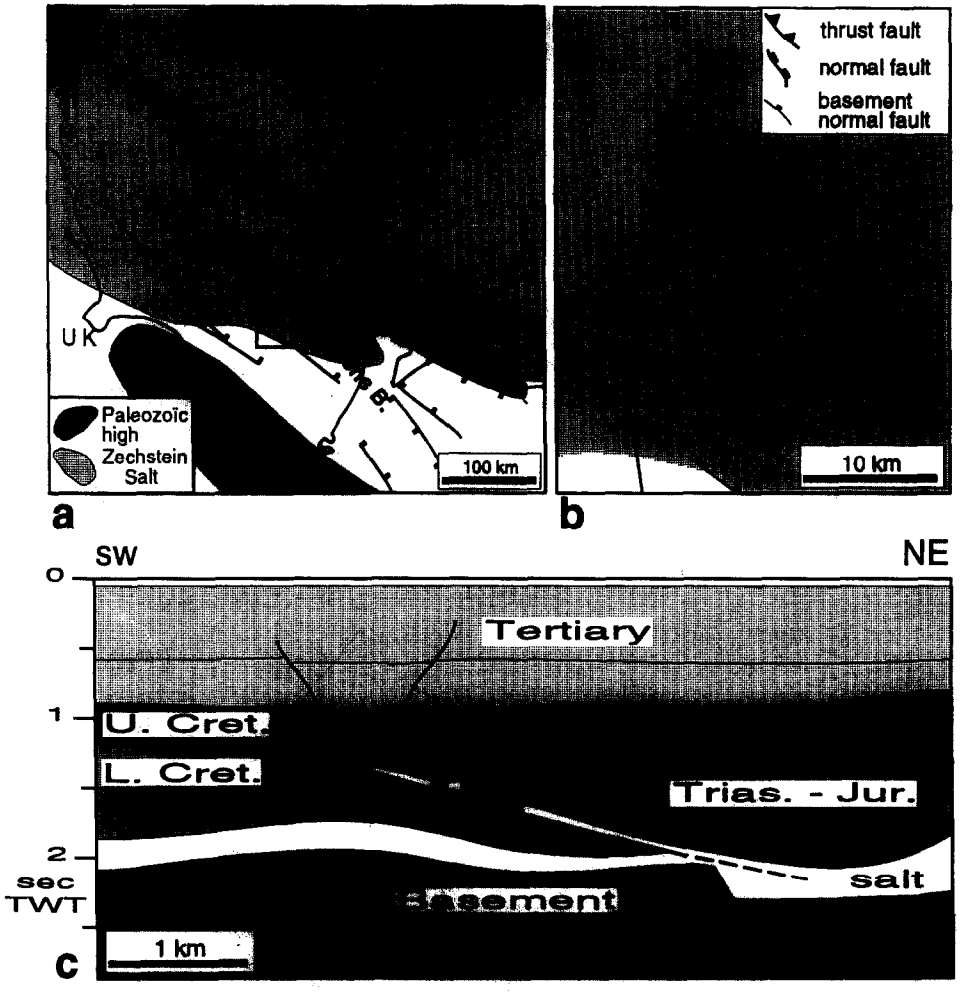

Fig. 3. Example of branching at depth of normal faults onto a décollement level of a pre-existing thrust fault in the Broad Fourteens Basin (North Sea). (a) Location of the Broad Fourteen Basin (modified after Ziegler 1990); (b) location of the newly-formed normal faults inside the basin; (c) line-drawing.

most accretionary wedges (see e.g. fig. 17 of Davis *et al.* 1983). Moreover, the rate of displacement has been chosen in order to obtain a strength profile for the décollement level analogous to the one calculated for a salt level (Nalpas & Brun 1993). Finally in both sets of experiments, a 5 cm-wide and 1 cm-thick strip of silicone putty is placed at the base of the sand-pack along the VD (Fig. 4 and Table 1) to avoid excessively restrictive control of fault location by the VD.

Models were run in two steps: first by compression producing thrust faults, and then extension producing normal faults. Compression is applied to the model at a variable angle (α) between the direction of compression and the VD direction (Fig. 4). Each set of experiments is made up of at least six models grading from pure compression ($\alpha = 90°$) to a strike-slip regime ($\alpha = 3°$), in order to obtain variable dips for the compressional faults (see Richard & Cobbold 1990). Later extension is always applied perpendicularly to the VD. In the second set of experiments, a thin layer (1 cm) of fresh sand is

Table 1. Main parameters of the materials used and the experimental procedure. Symbols for the parameters: ρ = density (g cm^{-3}), θ = angle between the fault plane and σ_1-axis, h = thickness, L = width, η = viscosity (measurement of viscosity was performed at 25°C, but experiments were performed at room temperature of 20°–25°C).

Set	Sand before comp.	Sand after comp.	Basal silicone	Interlayered silicone	Comp. velocity	Ext. velocity	α (angle of comp.)
I	$\rho = 1.6$ $\theta = 28°$ $h = 7$ cm	$\rho = 1.7$ $\theta = 24°$ $h = 7$ cm	$\eta = 10^4$ Pa s $p = 1.4$ $h = 1$ cm $L = 5$ cm	—	1 cm h^{-1}	1 cm h^{-1}	3°, 15° 23°, 30°
II	$\rho = 1.6$ $\theta = 28°$ $h = 7.5$ cm	$\rho = 1.7$ $\theta = 24°$ $h = 8.5$ cm	$\eta = 10^4$ Pa s $\rho = 1.4$ $h = 1$ cm $L = 5$ cm	$\eta = 10^3$ Pa s $\rho = 1.3$ $h = 0.5$ cm $L = 30$ cm	0.5 cm h^{-1}	0.25 cm h^{-1}	45°, 90°

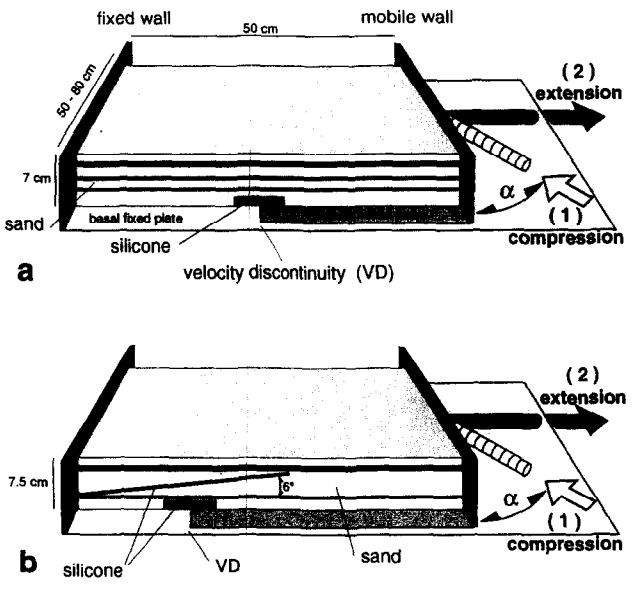

Fig. 4. Experimental apparatus used for the first (a) and for the second (b) set of experiments.

sieved onto the surface before extension in order to preserve the topography of the compressional structures.

Both compression and extension are interrupted at the first appearance of related faults. At the end of the experiment, the central part of the model is wetted and cut into serial sections perpendicular to the VD in order to examine the deformation pattern and measure fault dips. In the case of listric normal faults, dip is measured in the upper (β'—at the surface), middle (β'') and lower parts of the fault (β'''—top of the silicone layer).

Results—Set I

After compression the models are characterized by at least one thrust fault, or by a conjugate set of thrust and back-thrust faults (Fig. 5). Under pure compression ($\alpha = 90°$), thrust planes display a roughly planar geometry with an average dip of 30°, whereas back-thrusts show an average slightly steeper dip of 33°. At the base of the thrust plane, a slice of silicone putty a few mm thick and a few mm long penetrates into the fault zone. A plot of experimental data shows the increase of thrust and back-thrust dip as a function of decreasing of α angle (Fig. 5). Moreover, with a decrease of the α angle ($\alpha \leq 45°$), thrust and back-thrusts are arranged 'en échelon' (Fig. 6b').

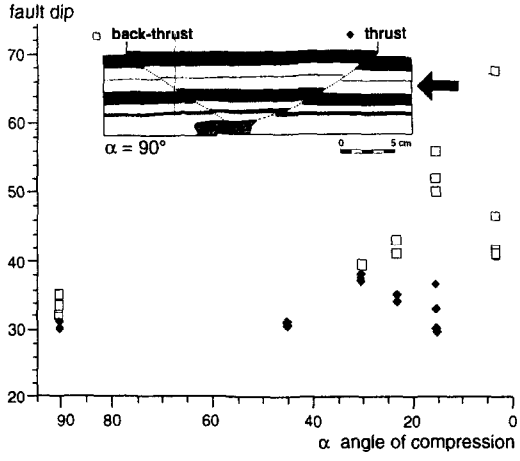

Fig. 5. Plot of fault dip (thrusts and back-thrusts) versus angle of compression (α), grading from a pure compressive regime to a strike-slip regime in the first set of experiments. The cross-section illustrates structures formed at the end of compression in the first set of experiments driven at $\alpha = 90°$.

During subsequent extension, a main normal fault develops at first but, as observed in compression, an antithetic normal fault may then appear. The increase of the dip of the thrust fault causes a change in the geometry of the normal faults as follows:

- when the thrust dip is less than 32° ± 1°, the main normal fault displays a listric geometry and is located in the centre of the basal silicone strip just above the VD (Figs. 6a and 7a);
- when the thrust dip increases above a critical value of 32° ± 1°, normal fault branches out from the base of the pre-existing thrust at the basal silicone/sand interface. This normal fault displays an approximately planar geometry (Figs. 6b and 7b). The main normal fault is always located at the rear of the thrust or at the rear of the back-thrust, when the compressive structures are arranged 'en échelon' (Fig. 6b');
- when the dip of the thrust planes reaches a critical dip value of 41° ± 1°, thrust faults are reactivated (Fig. 8). Due to the steeper dips, reactivation occurs preferentially on back-thrust faults during the early stages of extension. Then a conjugate normal fault develops at the rear of the thrust fault (Fig. 8a).

Results—Set II

The presence of an interlayered décollement level during compression produces a ramp and flat geometry (Figs. 6c and 9). At early stages of compression, a blind anticline structure develops above the basal ramp, and later a 'pop-up' structure appears at the upper termination of the décollement level (Figs. 6c' and 9). The minimum observed thrust dip is around 32° (Fig. 9). As observed in the previous set of experiments (Fig. 5), the dip of the thrust and back-thrusts (Fig. 9) as well as the basal ramp dip, increases with decreasing values of α angle. The increase of the basal ramp dip causes a backward migration of the related anticline. Moreover, during the final stage of deformation of experiment driven at $\alpha < 23°$, dextral strike-slip Riedel-like features appear inside the pop-up structure (Fig. 6d') (see also Naylor *et al.* 1986, Richard & Cobbold 1990).

During the early stages of extension, a ramp syncline appears above the basal ramp, which causes a smoothing of the pre-existing ramp-anticline. Afterwards, one or two conjugate normal faults develop inside the pop-up structure (Figs. 6c'' and 10a). Normal faults develop above the basal silicone strip, connected to the décollement level and cutting through the pop-up structure (Figs 6c and 10a). It is important to point out that reactivation of the décollement level occurs only at low

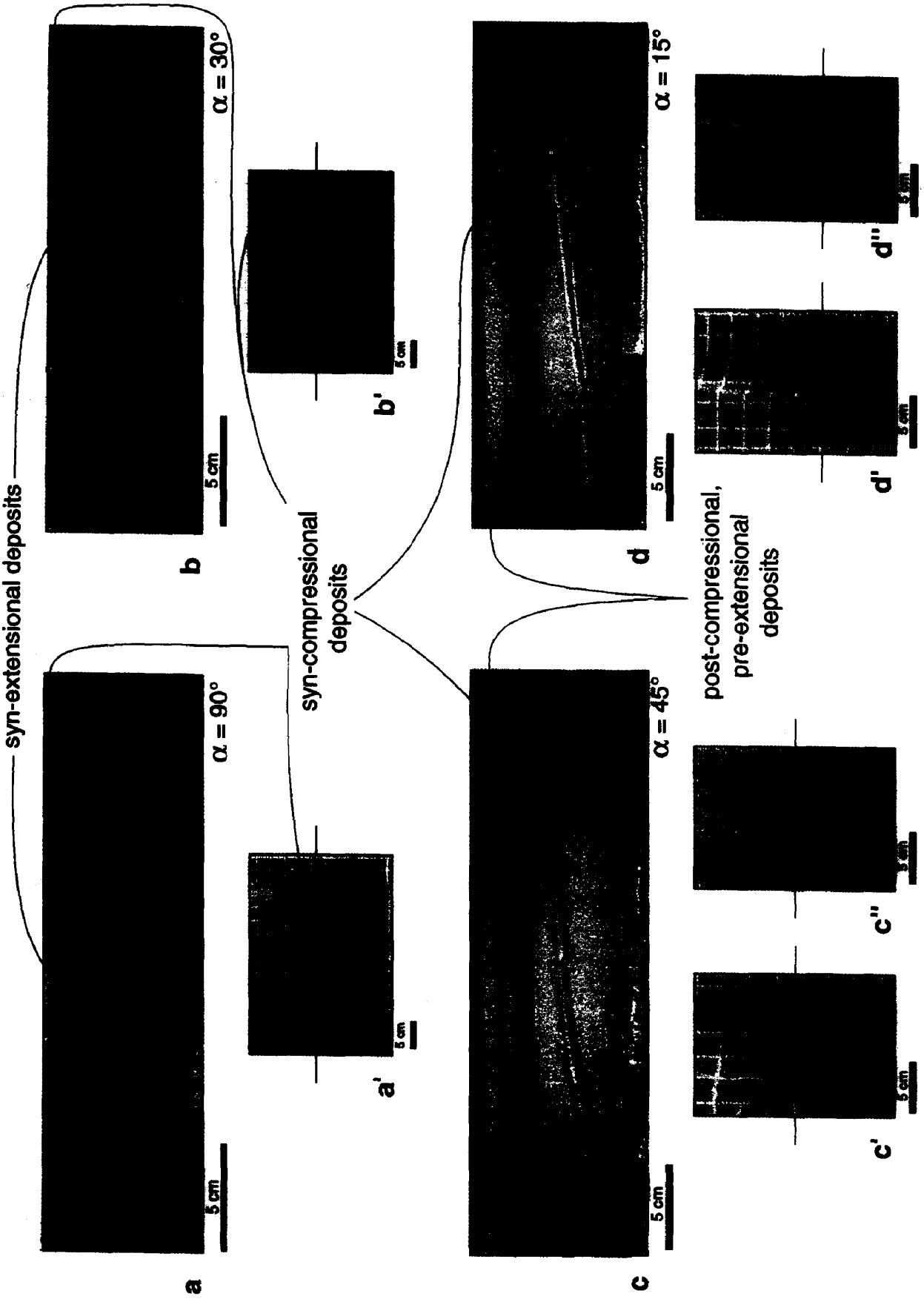

Fig. 6. Cross-sections and related top views of the first (a)–(b) and second (c)–(d) set of experiments. The traces of the cross-sections are marked on the top views. Moreover, the traces of the normal faults are outlined on the top views (a') & (b'). Top views (c') & (d') show the end of the extension phase, before sand sieving, while (c'') & (d'') were taken at the end of compression. Note that in the cross-section (a), antithetic normal fault cross-cuts a 31° dipping back-thrust fault.

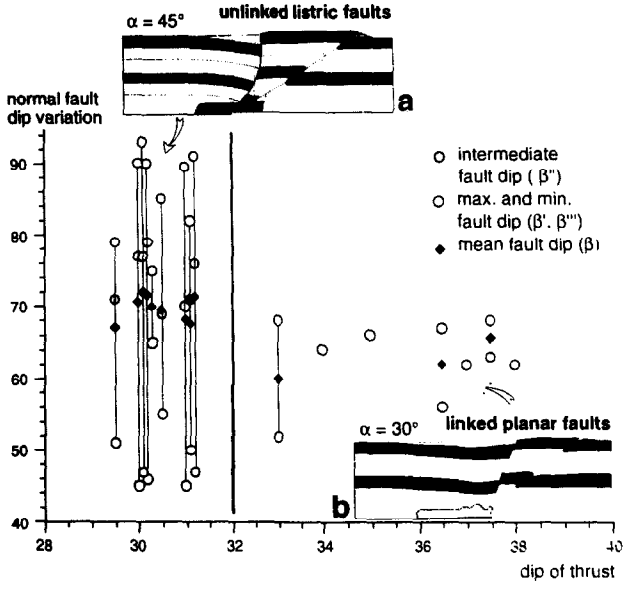

Fig. 7. Variation in normal fault-dip as a function of thrust dip. The interval between the minimum and the maximum dip of each normal fault is plotted vs the dip of the thrust. Listric normal faults (a), not linked to thrust planes (average values: $\beta' = 90°$, $\beta'' = 73°$, $\beta''' = 48°$, $\beta = 70°$), become closely linked to thrust planes when the thrust fault is steeper than 32° ± 1°, changing its geometry (b). A listric fault is defined in this study as a fault having minimum and maximum dips differing by more than 20°. Intermediate fault dip is measured in the central part of the model (at a height of 3 cm from the top of the basal silicone layer).

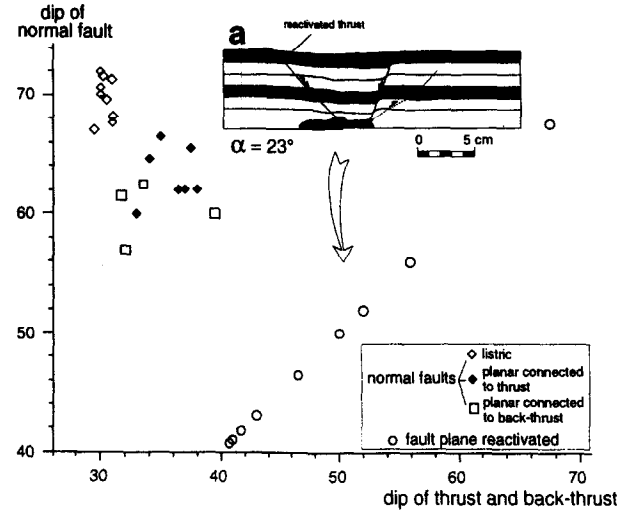

Fig. 8. Dip of the thrust and back-thrust vs dip of the normal fault in the first experimental set. In the case of listric faults, the mean of the three values is plotted ($\beta = \beta' + \beta'' + \beta'''/3$—see Fig. 7 for the minimum and maximum dip value). Reactivation occurs at dips of more than 41° ± 1°. The cross-section of a model driven at $\alpha = 23°$ indicates that reactivation occurs preferentially on back-thrusts.

displacement velocity (0.25 cm h^{-1}); in models driven at 0.5 cm h^{-1}, normal faults are seen to cross-cut the décollement level. The shape of the normal faults is relatively constant with a near-planar geometry (mean value of β'–β''' is around 20°); they are located at the rear of thrust faults, branching out from the silicone intruded at the base of the thrust. The dip of the normal faults is strongly influenced by the dip of the thrust: an increase

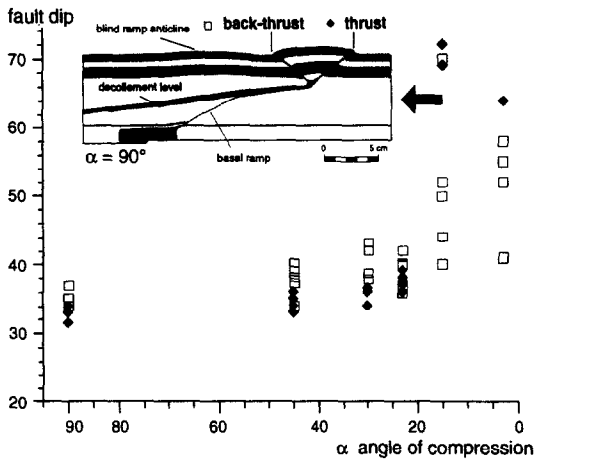

Fig. 9. Dip of thrusts and back-thrusts vs angle of compression (α), grading from a pure compressive to a strike-slip regime in the second set of experiments. The cross-section illustrates structures formed at the end of compression for the second set of experiments driven at $\alpha = 90°$.

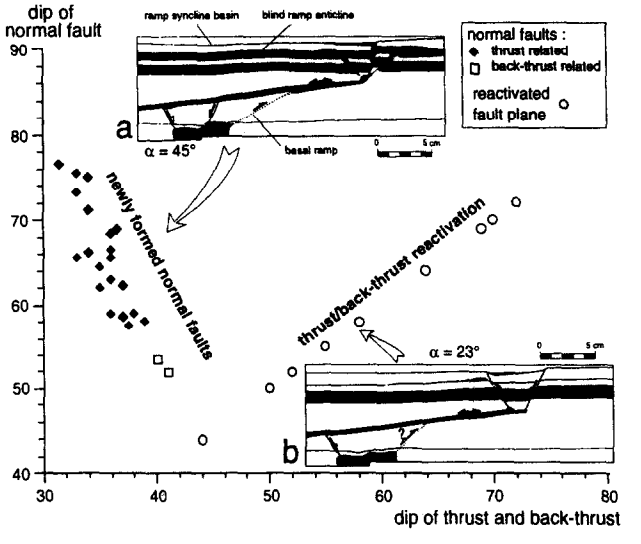

Fig. 10. Dip of the thrust and back-thrust vs dip of the normal faults in the second set of experiments. A linear regression is observed between the dip of the thrusts and the dip of the associated normal faults. Insert (a) & (b) contain line drawings of two cross-sections for models driven with $\alpha = 45°$ and 23°, respectively.

of thrust fault dip of 6°–8° causes a decrease in the dip of normal faults of more than 15° (Fig. 10). Finally, reactivation of the upper thrust ramp is similar in type to that observed in the first set of experiments and occurs preferentially on the back-thrust planes (Figs. 6d and 10b). The observed minimum angle of reactivation is around 44°, but no data are available for the 41°–44° interval.

Interpretation

Sand models without a basal silicone layer, driven only in extension (Vendeville *et al.* 1987) or in compression and extension (Krantz 1991b), show normal faults with a quasi-planar geometry. Local steepening confined to the upper part of the fault is due to the sand dilatancy (Mandl 1988); local flattening in the lower part

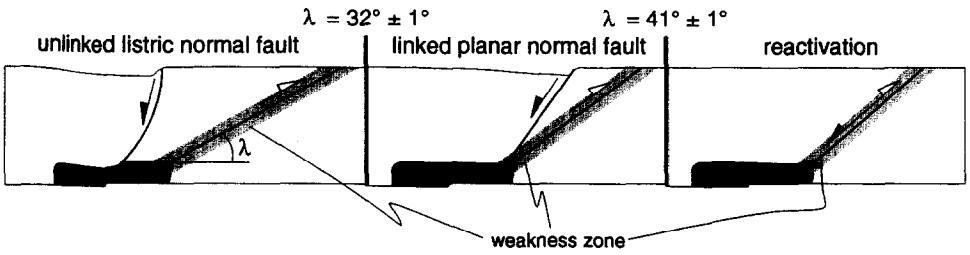

Fig. 11. Sketch of the geometrical relationships between a hypothetical pre-existing weakness zone and newly-formed normal faults. In the first case ($\lambda < 32° \pm 1°$, where λ is the dip of the thrust plane), listric normal faults are not linked to the thrust plane. For an angle $\lambda > 32° \pm 1°$, interaction between the normal fault and the weakness zone increases, while normal faults branch out from the base of the thrust at the interface with the décollement; the geometry of the fault is planar. For angles $\lambda > 41° \pm 1°$, complete reactivation occurs.

of the fault is controlled by the basal friction. In a similar way, models with a continuous basal silicone layer frequently show planar normal faults (Allemand *et al.* 1989). In our models with a silicone layer of finite width, listric normal faults are able to develop. In extension, the basal silicone layer thins more heterogeneously above the VD in comparison to models with a continuous basal silicone layer, thus inducing an asymmetric and localized flexure of the sand-pack. This is believed to cause a bending of the principal stress trajectories (Sanford 1959, Horsfield 1977, Vendeville 1987, Mandl 1988). The rotation of the principal stress axes allows the dip angle β' of the upper part of the fault to reach a value of 90° or more, causing a vertical or reverse displacement along the fault near the surface (Figs. 6a and 7a). As a result, a listric normal fault develops with a hanging wall roll-over anticline. In our models with a basal silicone layer, listric geometry is only observed when normal faults develop within undeformed sand [test model driven only in extension; Nalpas (in press)] or near a pre-existing thrust fault with a dip of less than 32° ± 1° (Figs. 6a and 11). When the dip of the thrusts reaches an angle of 32° ± 1°, normal faults branch out near the base of the thrust faults (Figs. 6b, 7b and 11). In this case, normal faults develop with a planar geometry at the rear of the thrusts. Then, the location and the geometry of normal faults are influenced by the presence of the pre-existing thrust faults where a drop in shear strength due to the sand dilatancy is likely to occur (Mandl *et al.* 1977, see also Appendix). In the second set of experiments, normal faults always branch out near the bases of thrust faults (Figs. 6c and 10a), which show dips steeper than 32° ± 1°. We observe that the dip of newly-formed normal faults progressively decreases with increasing dip of pre-existing thrust faults (Fig. 10). Similar phenomena have been observed in sand models (Krantz 1991b, Küntz 1994) and are believed to be due to the presence of a pre-existing zone of weakness. In this study, we suggest that the change of the normal fault dip is due to a drop in frictional coefficient near a pre-existing zone of weakness (see Appendix). As proposed for natural examples (Zoback 1991, Zoback & Zoback 1991), the presence of a zone of weakness could induce rotation of the principal stress axes. In extension, the maximum compressive stress gradually rotates from the vertical towards the dip of the weak pre-existing structure (Ben-Avraham & Zoback 1992). The amount of rotation of the σ_1-axis is related to the angle between the pre-existing weak structure (thrust plane) and the theoretical vertical σ_1-axis; the more this angle decreases—i.e. as thrust dip increases—the more the σ_1-axis rotates, until a critical value is reached (Zoback & Zoback 1991).

Finally, when thrust planes reach a dip of about 41° ± 1°, total reactivation occurs (Figs. 6d, 8a, 10b and 11). This observed minimum critical angle of reactivation is in agreement with theoretical calculations (see Appendix) and with previous sand models (Krantz 1991b). Even this process could be due to a drop in the frictional coefficient along the weakness zone (see Appendix), occurring mainly in the early stages of extension. Furthermore, in the second set of experiments, extensional re-working of the silicone décollement level occurs only when a low rate of displacement, i.e. low shear strength, is imposed.

DISCUSSION AND CONCLUSIONS

The results of analogue modelling give some insights into the mechanical aspects of the interactions between newly-formed normal faults and pre-existing thrust faults.

(a) The results of our experiments and observations from the Central Apennines indicate that normal faults only slightly interact—if at all—with shallow-dipping pre-existing thrust faults. In this case, the location and the geometry of the normal faults seem to be unaffected by the thrust faults.

(b) The branching at depth of normal faults onto thrust planes occurs preferentially at the termination of a décollement level and induces a control upon the geometry of the normal faults. Experimental results indicate that, when the dip of the pre-existing thrust reaches a critical angle (32° ± 1°), normal faults branch out from the base of the thrust fault at the interface with the ductile décollement. The observations in the Broad Fourteens Basin are supported by these results, since normal faults branch out from the thrust fault at the termination of the evaporite décollement level. In this case, the location of the normal faults are controlled by the inherited configuration of the décollement level.

The dip of the newly-formed normal faults may be

also controlled by the presence of a pre-existing thrust plane. In our model, when branching at depth occurs, the dip of normal faults decreases following an increase in the dip of the thrust plane. We suggest that this phenomenon is due to the presence of a pre-existing zone of weakness where shear strength decreases and the principal stress axes are rotated. This relation may offer a further explanation to the observation that very shallow-dipping normal faults [less than 30°; cf. Jackson (1987)] are recognized especially in areas of previous thickening and thrusting (e.g. Brun & Choukroune 1983).

(c) In both model and nature, the extensional reactivation of a thrust fault depends upon its shear strength. In dry sand, with a frictional angle of about 24°, complete extensional reactivation of a pre-existing thrust fault occurs only when the thrust plane dips at more than 41° ± 1°. We propose that this observed minimum critical angle of reactivation depends upon the drop in friction coefficient, and thus in shear strength, that occurs along a pre-existing faulted zone. In the brittle crust, the geometry of pre-existing thrust planes, the coefficient of friction, the cohesion and pore pressure are fundamental parameters which control fault reactivation. Accordingly, observations from the Central Apennines imply that the dip of the pre-existing thrust fault is indeed an important parameter controlling superficial reactivation processes. Even though reactivation of lower angle thrust planes is possible (e.g. Ratcliffe *et al.* 1986), this would require a major influence of the parameters mentioned above (e.g. Sibson 1985). As illustrated by the Broad Fourteens Basin (Fig. 2), the extensional reactivation of thrust faults connected to gently-dipping décollement level is commonly observed. Our experimental results indicate the reactivation of a 5°–6° dipping décollement. In such cases, the reactivation is strongly dependent on the shear strength of the décollement layer, which for a given viscosity of the layer rocks is controlled by the strain rate. At high strain rates, a layer made of very weak rocks (e.g. salt) can be cross-cut by normal faults.

Acknowledgements—We would like to thank Jean-Jaques Kermarrec for his invaluable assistance during laboratory experiments and to Jean-Charles Thomas for improving an early version of the manuscript. C. Faccenna is grateful to Renato Funiciello and to Jean-Paul Cadet for the scientific support, to Francesco Salvini for useful discussions and to Marc de Urreiztieta for logistical support. We are especially grateful to Dimitrios Sokoutis, who substantially improved the manuscript. We thank ELF Petroland for authorization to publish the Broad Fourteen Basin Section. The financial support of C. Faccenna is provided by CNR grant number 203.05.15. M. S. N. Carpenter was responsible for editing the English style.

APPENDIX

Dry Fontainebleau sand (quartzose, well sorted and well rounded-grains) was introduced and levelled in the experimental apparatus, being sieved with a 0.5 mm mesh from a height of 40 cm. This technique gives a density of 1.60–1.62 to the sand-pack. Several test models, driven in compression and in extension only, were performed to define the angle θ between the fault plane trace and the principal stress axis σ_1. Fault dip measurements yield an average of $\theta = 28°$.

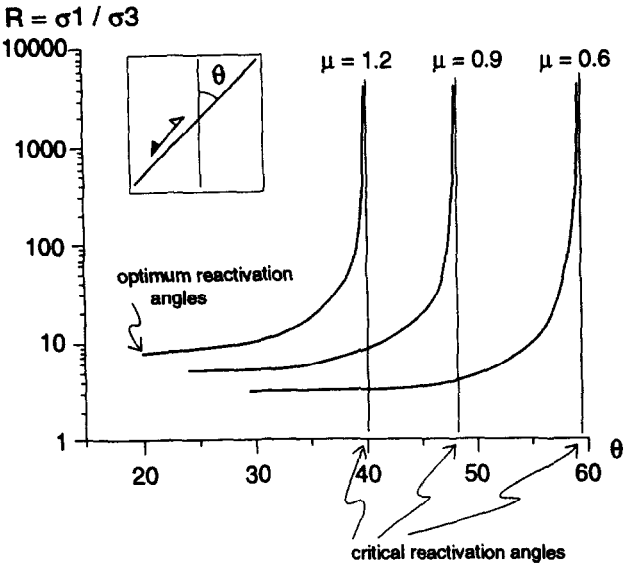

Fig. A1. Stress ratio (R) versus the angle between the fault plane and the σ_1-axis (θ) for different friction coefficients. The diagram shows that a critical reactivation angle of 41.5° occurs for a sand with a friction coefficient of 0.9.

To model extensional reactivation of pre-existing thrust faults, we performed a two-stage run consisting firstly of compression and then extension. A certain degree of compaction is preserved by the sand at the end of compression, and the observed θ angle decreases to about 24°. The coefficient of internal friction (μ), as expressed by Anderson (1951), is given by:

$$\mu = \tan(2\theta - 90°) = \tan \phi, \quad \text{(A1)}$$

where ϕ is the angle of internal friction (42°). This equation yields a μ value of 0.9. The stress ratio (R) necessary to reactivate a pre-existing plane with variable dip is given by the following relation (Sibson 1985):

$$R = \sigma_1/\sigma_3 = (1 + \mu \operatorname{cotg}\theta)/(1 - \mu \operatorname{tg}\theta). \quad \text{(A2)}$$

For the above parameter ($\mu = 0.9$), the minimum dip of the pre-existing reactivated plane is of 41°–42° (Fig. A1). This value is in good agreement with the models of Krantz (1991b) as well as the results presented here.

As described by Mandl *et al.* (1977), the uncompacted sand reaches the rupture peak through a softening process that causes the formation of a narrow dilatancy zone whose width depends upon the initial density of the material.

From equation (A2) we also obtain:

$$\sigma_3 = 0.19\ \sigma_1. \quad \text{(A3)}$$

At a depth of 6 cm, assuming a density of 1.7, the differential stress σ_1–σ_3 is ≈810 Pa (Fig. A2b). The construction of the Mohr circle, assuming a cohesionless material, allows us to trace a failure envelope for the intact sand and for reactivation of the pre-existing anisotropy (Fig. A2a). This envelope corresponds to an angle of internal friction (ϕ^*) fixed by the experimental and theoretical value of 32°, and a related friction coefficient $\mu^* = 0.6$.

The stress ratio for reactivation (R^*) has a minimum positive value (Sibson 1985):

$$R^* = ((1+\mu^{*2})^{1/2}+\mu^*)^2, \quad \text{(A4)}$$

which, for the above values gives $R^* = 3.1$.

In an extensional regime, the differential stress required to reactivate a pre-existing anisotropy (Ranalli & Yin 1990) is given as follows:

$$\sigma_1^* - \sigma_3^* = ((R-1)/R)(\rho g z)(1-\lambda), \quad \text{(A5)}$$

yielding a value of 677 Pa, where z is the depth and λ the pore pressure, equal to zero in our models (Fig. A2b).

Finally, we propose that, assuming a cohesionless sand, reactivation processes can be explained by a fall in the friction coefficient within the dilatancy zone (Fig. A2b). From our experiments we estimate a drop in friction coefficient of about 30%.

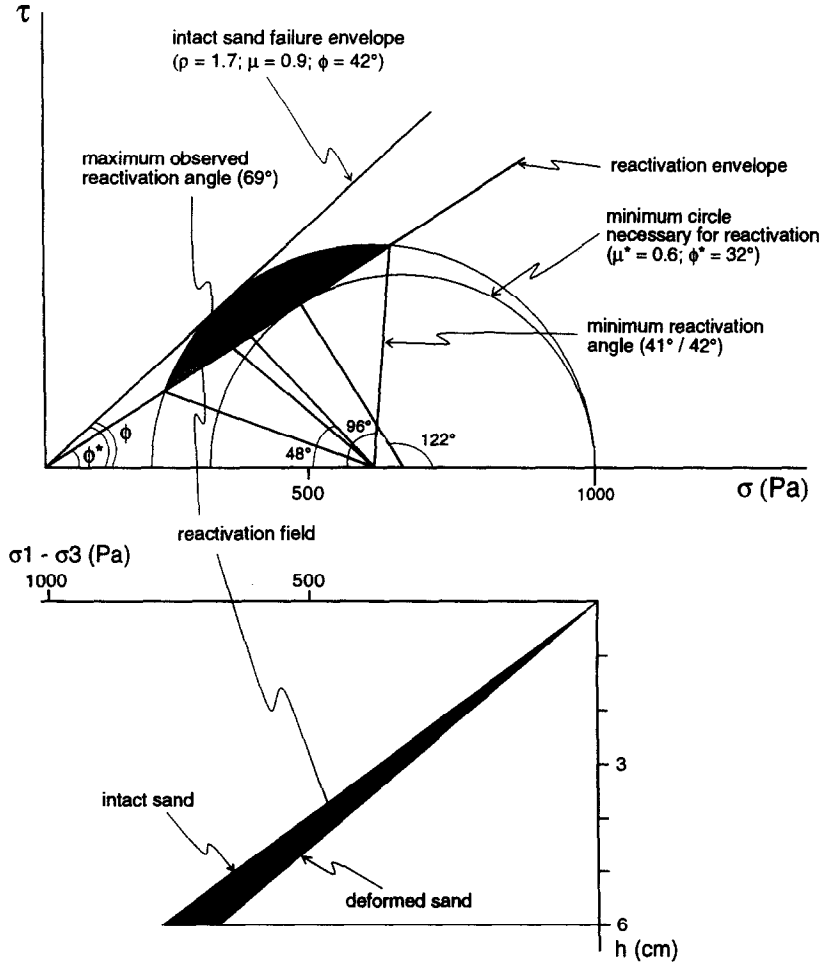

Fig. A2. Mohr circles for stress (at a depth of 6 cm) and a related shear strength profile for the intact sand and reactivated planes (main parameters for the sand used are $\mu = 0.9$ and $\rho = 1.7$).

REFERENCES

Allemand, P., Brun, J.-P., Davy, P. & Van den Driessche, J. 1989. Symétrie et asymétrie des rifts et mécanisme d'amincissements de la lithosphère. *Bull. geol. Soc. Fr.* **8**, 445–451.

Allmendinger, R. W., Sharp, J. W., Von Tish D., Serpa, L., Brown, L., Kaufmans, S., Olivier, J. & Smith, R. B. 1983. Cenozoic and Mesozoic structures of the Eastern Basin and Range province, Utah, from COCORP seismic reflection data. *Geology* **11**, 532–536.

Anderson, E. M. 1951. *The Dynamics of Faulting*. Oliver & Boyd, Edinburgh.

Arabasz, W. J. & Julander, D. R. 1986. Geometry of the seismic active faults and crustal deformation within the Basin and Range-Colorado Plateau transition in Utah. In: *Extensional Tectonics of the Southwestern United States: a Perspective on Processes and Kinematics* (edited by Mayer, L.). *Geol. Soc. Am.*, **208**, 43–75.

Bally, A. W., Burbi, L., Cooper, C. & Ghelardoni, R. 1986. Balanced cross-section and seismic problems across the Central Apennines. *Mem. geol. Soc. d'It.* **35**, 257–310.

Ben-Avraham, Z. & Zoback, M. D. 1992. Transform-normal extension and asymmetric basins: an alternative to pull-apart models. *Geology* **20**, 423–426.

Bodenhausen, J. W. A. & Ott, W. T. 1982. Habitat of the Rijswijk Oil Province, Onshore. The Netherlands. In: *Petroleum Geology of the Continental Shelf of North-West Europe* (edited by Illing, L. V. & Hobson, G. B.). Institut of Petroleum, London, 301–309.

Bosi, V., Funiciello, R. & Montone, P. In press. Fault inversion: an example in Central Apennines (Italy). *Il Quaternario*.

Brewer, J. A. & Smythe, D. K. 1984. MOIST and the continuity of crustal reflector geometry along the Caledonian-Appalachian orogen. *J. geol. Soc. Lond.* **141**, 105–120.

Brun, J.-P. & Choukroune, P. 1983. Normal faulting, block tilting and décollement in a stretched crust. *Tectonics* **2**, 345–356.

Chadwick, R. A., Kenolty, N. & Whittaker, A. 1983. Crustal structure beneath southern England from deep seismic reflection. *J. geol. Soc. Lond.* **140**, 893–912.

Cheadle, M. J., McGreany, S., Warner, M. R. & Matthews, D. H. 1987. Extensional structures in the western UK continental shelf: a review of evidence from deep seismic profile. In: *Continental Extensional Tectonics* (edited by Coward, M. P., Dewey, J. F. & Hancock, P. L.). *Spec. Publ. Geol. Soc.* **28**, 445–456.

Cooper, C. & Burbi, L. 1986. Geology of the Central Sibillini Mountains. *Mem. geol. Soc. It.* **35**, 323–347.

Davis, D., Suppe, J. & Dahlen, F. A. 1983. Mechanics of fold and thrust belts and accretionary wedges. *J. geophs. Res.* **88**, 1153–1172.

Davy, P. & Cobbold, P. R. 1991. Experiments on shortening of a 4-layer model of the continental lithosphere. In: *Experimental and numerical modelling of continental deformation* (edited by Cobbold, P. R.). *Tectonophysics* **188**, 1–25.

Davy, P. 1986. *Modélisation thermomécanique de la collision continentale*. Mem. et doc. du Centre Armorican d'Etude Structurale des socles, **8**, 1–233.

Donath, F. P. & Cronwell, R. M. 1981. Probabilistic treatment of faulting in geologic media. In: *Mechanical Behavior of Crustal Rocks* (edited by Carter, N. L., Friedman, M., Logan, J. M. & Strarns, D. W.). *Am. Geophys. Un. Geophys. Monogr.* **24**, 231–241.

Enfield, M. & Coward, M. 1987. The structures of western Orkney Basin, northern Scotland. *J. geol. Soc. Lond.* **144**, 871–884.

Funiciello, R., Parotto, M. & Praturlon, A. 1981. Carta tettonica d'Italia 1:1.500.000. P.F.G.-C.N.R., Roma.

Ghisetti, F., Barchi, M., Bally, I. W., Moretti, I. & Vezzani, L. 1993. Conflicting balanced structural section across the Central Apennines (Italy): problems and implications. In: *Generation, Accumulation and Production of Europe's Hydrocarbons III* (edited by Spencer, A. M.). *Spec. Publ. Euro. Ass. Petrol. Geosci.* **3**, 219–231.

Gibbs, A. D. 1987. Basin development, examples from United Kingdom and comments on hydrocarbon prospectivity. *Tectonophysics* **133**, 189–198.

Gorini, C., Viallard, P. & Deramond, J. 1991. Modèle d'inversion structurale négative: la tectonique extensive post-nappe du fossé de Narbonne–Sigean (Corbières, Sud de la France). *C. r. Acad. Sci. Paris* t **312**, 1013–1019.

Horsfield, W. T. 1977. An experimental approach to basement-controlled faulting. *Geologie Mijnb.* **56**, 363–370.

Hubbert, M. K. & Rubey, W. W. 1959. Role of fluid pressure in mechanics of overthrusting faulting. *Bull. geol. Soc. Am.* **70**, 115–166.

Huyghe, P. & Mugnier, J. L. 1992. The influence of depth on reactivation in normal faulting. *J. Struct. Geol.* **14**, 991–998.

Ivins, E. R., Dixon, T. H. & Golombek, M. P. 1990. Extensional reactivation of an abandoned thrust: a bound on shallowing in the brittle regime. *J. Struct. Geol.* **12**, 303–314.

Jackson, J. A. 1987. Active normal faulting. In: *Continental Extensional Tectonics* (edited by Coward, M. P., Dewey, J. F. & Hancock, P. L.). *Spec. Publ. geol. Soc.* **28**, 551–558.

Jolivet, L., Daniel, J. M. & Fournier, M. 1991. Geometry and kinematics of the Alpine Corsica. *Earth Planet. Sci. Lett.* **104**, 278–291.

Krantz, R. W. 1991a. Measurement of friction coefficients and cohesion for faulting and fault reactivation in laboratory models using sand and sand mixtures. In: *Experimental and Numerical Modelling of Continental Deformation* (edited by Cobbold, P. R.). *Tectonophysics* **188**, 203–207.

Krantz, R. W. 1991b. Normal faults geometry and fault reactivation in tectonic inversion experiments. In: *The Geometry of Normal Faults* (edited by Roberts, A. M., Yielding, G. & Freeman, B.). *Spec. Publ. geol. Soc.* **56**, 207–217.

Küntz, M. 1994. Approche expérimentale de la déformation dans le systèmes préfracturés: une application à l'inversion tectonique des bassins sedimentaires. Thèse d'Université, Rennes.

Lavecchia, G., Minelli, G. & Pialli, P. 1987. Contractional and extensional tectonics along the transect Trasimeno Lake-Pesaro (Central Italy). In: *The Lithosphere in Italy. Advances in Earth Science Research* (edited by Boriani, A., Bonafede, M., Piccardo, G. B. & Vai, G. B.). *Atti Convegno Lincei* **80**, 139–142.

Malavielle, J. 1987. Kinematics of compressional and extensional ductile shearing deformation in a metamorphic core complex of the North-Eastern Basin and Range. *J. Struct. Geol.* **9**, 541–554.

Mandl, G. 1988. *Mechanics of Tectonic Faulting—Models and Basic Concepts*. Development in Structural Geology **1** (series editor Zwart, H. J.), Elsevier.

Mandl, G., De Jong, L. N. J. & Maltha, A. 1977. Shear zones in granular material. *Rock Mech.* **9**, 95–144.

Mariotti, G. & Capotorti, F. 1988. Analisi ed interpretazione di alcuni elementi tettonici recenti nella media valle del Salto (Rieti). *Rend. Soc. Geol. It.* **11**, 78–94.

Nalpas, T. & Brun, J.-P. 1993. Salt flow and diapirism related to extension at crustal scale. *Tectonophysics* **228**, 349–362.

Nalpas, T. 1994. Inversion de graben du Sud de la Mer du Nord. Données de sub-surface et modélisation analogique. Thèse Université de Rennes I.

Nalpas, T., Le Douaran, S., Brun, J.-P., Unternehr, P. & Richert, J.-P. In press. Inversion of the Broad Fourteens Basin (offshore netherlands). A small scale investigation. *Sediment. Geol.*

Naylor, M. A., Mandl, G. & Sijpestein, C. H. K. 1986. Fault geometries in basement-induced faulting under different initial stress states. *J. Struct. Geol.* **8**, 737–752.

Nijman, W. 1971. Tectonics of the Velino-Sirente area, Abruzzi, Central Italy. *Koninkl. Nederl. Akad. Van Wetenschappen Proc.* **B74**, 156–184.

Parotto, M. & Praturlon, A. 1975. Geological summary of Central Apennines. In: *Structural Model of Italy* (edited by Ogniben, L., Parotto, M. & Praturlon, A.). *Quad. Ric. Scient.* **90**, 257–331.

Petersen, T. A., Brown, L. D., Cook, F. L., Kaufman, S. & Oliver, J. E. 1984, Structure of the Rideville basin from COCORP seismic data and implication for reactivation tectonics. *J. Geol.* **92**, 261–271.

Powell, C. M. & Williams, G. D. 1989. The Lewis/rocky Mountain trench fault system in Northwest Montana, USA: an example of negative inversion tectonics? In: *Inversion Tectonics* (edited by Cooper, M. A. & Williams, G. D.). *Spec. Publ. geol. Soc.* **44**, 223–234.

Ranalli, G. & Yin, Z. M. 1990. Critical stress difference and orientation on faults in rocks with strength anisotropies: the two dimensional case. *J. Struct. Geol.* **12**, 1067–1071.

Ratcliffe, N. M., Burton, W. C., D'Angelo, R. M. & Costain, J. K. 1986. Low-angle extensional faulting, reactivated mylonites, and seismic reflection geometry of the Newark basin margin in eastern Pennsylvania. *Geology* **14**, 766–770.

Richard, P. & Cobbold, P. R. 1990. Experimental insights into partitioning of fault motions in continental convergent wrench zones. *Annls Tecton.* **4**, 34–44.

Sanford, A. R. 1959. Analytical and experimental study of simple geological structures. *Bull. geol. Soc. Am.* **70**, 19–52.

Seranne, M. & Seguret, M. 1987. The Devonian basin of Western Norvey, tectonics and kinematics in an extending crust. In: *Continental Extensional Tectonics* (edited by Coward, M. P., Dewey, J. F. & Hancock, P. L.) *Spec. Publ. geol. Soc.* **28**, 537–548.

Sibson, R. H. 1985. A note on fault reactivation. *J. Struct. Geol.* **7**, 751–754.

Sibson, R. H. 1990. Rupture nucleation on unfavourably oriented faults. *Bull. seism. Soc. Am.* **80**, 1580–1604.

Smith, R. B. & Bruhn, R. L. 1984. Intraplate extensional tectonics of the eastern Basin and Range: interferences of structural styles from seismic reflection data, regional tectonics, and thermal mechanical models of brittle–ductile deformation. *J. geophs. Res.* **89**, 5733–5762.

Stein, A. M. & Blundell, D. J. 1990. Geological inheritance and crustal dynamics of the northwest Scottish continental shelf. *Tectonophysics* **173**, 455–467.

Stoneley, R. 1982. The structural development of the Wessex basin. *J. geol. Soc. Lond.* **139**, 545–554.

Vendeville, B. C. 1987. Champs de failles et tectonique en extension. Mem. et doc. du Centre Armorican d'Etude Structurale des socles **15**, 1–395.

Vendeville, B. C., Cobbold, P. R., Davy, P., Brun, J.-P. & Choukroune, P., 1987. Physical models of extensional tectonics at various scale. In: *Continental Extensional Tectonics* (edited by Coward, M. P., Dewey, J. F. & Hancock, P. L.). *Spec. Publ. geol. Soc.* **28**, 95–107.

Weijermars, R. 1986. Flow behavior and physical chemistry of bouncing putty and related polymers in view of tectonic laboratory applications. *Tectonophysics* **124**, 325–358.

Wernicke, B. 1981. Low-angle normal faults in the Basin and Range Province-Nappe tectonics in an extending orogen. *Nature* **291**, 645–648.

Williams, G. D., Powell, C. M. & Cooper, M. A. 1989. Geometry and kinematics of inversion tectonics. In: *Inversion Tectonics* (edited by Cooper, M. A. & Williams, G. D.). *Spec. Publ. geol. Soc.* **44**, 3–15.

Yin, Z.-M. & Randalli G. 1992. Critical stress difference, fault orientation and slip direction in anisotropic rocks under non-Andersonian stress system. *J. Struct. Geol.* **14**, 237–244.

Ziegler, P. A. 1975. North Sea basin history and tectonic framework of North-Western Europe. In: *Petroleum and the Continental Shelf of North-West Europe* (edited by Woodland, A. W.). *Geology* **1**, 131–148.

Ziegler, P. A. 1990. Geological atlas of Western and Central Europe. Shell Internationale Petroleum Maatscappij B. V..

Zoback, M. 1991. State of stress and crustal deformation along weak transform faults. *Phil. trans. R. Soc. Lond.* **A 331**, 141–150.

Zoback, M. D. & Zoback, M. L. 1991. Tectonic stress field of North America and relative plate motions. In: *Neotectonics of North America* (edited by Slemmons, D. B., Engdahl, E. R., Zoback, M. D. & Blackwell, D. D.). *Geol. Soc. Am., Decade Map* **1**, 339–366.